Symmetry analysis of magneto-optical effects: The case of x-ray diffraction and x-ray absorption at the transition metal $L_{2,3}$ edge

M. W. Haverkort
Max Planck Institute for Solid State Research, Heisenbergstraße 1, D-70569 Stuttgart, Germany

N. Hollmann
II. Physikalisches Institut, University of Cologne, Zülpicher Straße 77, D-50937 Köln, Germany

I. P. Krug
Institut für Festkörperforschung IFF-9, Forschungszentrum Jülich GmbH, D-52425 Jülich, Germany

A. Tanaka
Department of Quantum Matter, ADSM, Hiroshima University, Higashi-Hiroshima 739-8530, Japan
(Received 9 October 2009; revised manuscript received 8 June 2010; published 1 September 2010)

A general symmetry analysis of the optical conductivity or scattering tensor is presented and used to rewrite the conductivity tensor as a sum of linear independent spectra multiplied by simple functions depending on the local magnetization direction. This allows one to describe the full, magnetization directional dependent, magneto-optical response of a system in arbitrary symmetry by only a few linear independent fundamental spectral functions. Using this formalism, we discuss the azimuthal dependence of the resonant x-ray diffracted intensity on magnetic Bragg reflections. We present several numerical examples at the transition metal $L_{2,3}$ edge. From these numerical calculations, we can conclude that for realistic parameters several fundamental spectra, not present in spherical symmetry, become important and should not be neglected. Deviations from the standard analysis in spherical symmetry become large in cases where orbital order coexists with magnetic order, even if the orbital order is at a different $\boldsymbol{q}$ vector. In the extreme case of the layered cuprates, one finds that one is not sensitive to the projection of the magnetic moments onto the plane of the ordered $d_{x^2-y^2}$ hole. Not including the correct crystal symmetry can lead to incorrectly determined magnetic orientations and structures.

DOI: 10.1103/PhysRevB.82.094403 PACS number(s): 78.20.Ls, 78.70.Ck, 78.70.Dm

Resonant x-ray diffraction or reflectivity (RXD) has developed into a powerful method to study charge, orbital, and magnetic ordering in transition metal compounds and artificially created superlattices. In principle, the resonant energy dependence of the scattering profile and its polarization and azimuthal dependence contain the information about the local magnetic, charge, and orbital order. Obtaining this information from such spectra is often still a theoretical and experimental challenge.

One of the more straightforward methods to analyze magnetic Bragg reflections has been presented by Hannon *et al.*[1] and several other authors.[2–8] They showed that the azimuthal intensity dependence can be related to the local orientation of the magnetic moment by a simple relation. The scattered intensity is proportional to $|(\boldsymbol{\varepsilon}_{in}\times\boldsymbol{\varepsilon}^{*}_{out})\cdot\hat{\boldsymbol{m}}|^2$, whereby $\boldsymbol{\varepsilon}_{in(out)}$ is the polarization of the incoming (outgoing) light and $\hat{\boldsymbol{m}}$ is a unit vector in the direction of the magnetization. These relations are used relatively often in the analyses of RXD nowadays.[9] The crux is that these relations are derived in spherical symmetry and strictly speaking hold only in spherical symmetry. An extended formalism has been presented[10–12] but not seen a large audience so far. The question the present paper addresses is; how large are the changes in the scattered intensity when the effects of the real crystal symmetry are included, when is it important to include the real crystal symmetry, and when one can still use the formulas derived in spherical symmetry. We will present a general symmetry analysis of the conductivity or scattering tensor including an arbitrary magnetization direction and several numerical calculations at the transition metal $L_{2,3}$ edge, in order to exemplify when deviations from spherical symmetry become important. We will restrict ourselves to dipole transitions only. For the numerical calculations, we will neglect the valence-band spin-orbit coupling. The spin-orbit coupling for the core orbitals (transition metal $2p$) is naturally included. This is in many cases a valid approximation as valence orbital momenta are often quenched. The numerical magneto-optical effects presented here are due to the core-hole spin-orbit coupling, which is at the transition metal $L_{2,3}$ edge quite large.

A hint for the importance of including the correct crystal symmetry might be obtained from absorption spectroscopy. By the optical theorem,[13] it is well known that the scattering tensor F and the conductivity tensor σ are related by a factor of ω ($F\propto\omega\sigma$). Therefore all magneto-optical effects known from absorption spectroscopy should return in diffraction or reflectivity experiments. Recently it has been realized that the symmetric part of the conductivity tensor due to magnetism i.e., the magnetic linear dichroism effect is not given by a single spectrum as in spherical symmetry but behaves more complicated in cubic or lower symmetries.[14–17] For an antiferromagnetic Bragg reflection, the symmetric part of the scattering tensor does not contribute to the diffracted intensity. How the antisymmetric part of the conductivity tensor

behaves for less than spherical symmetry is not well known in the x-ray regime. For infrared and visible wavelengths, there are several experiments and numerical calculations showing that for systems with less than cubic symmetry, the magnetic part of the optical conductivity tensor σ becomes considerably different from what is expected in spherical symmetry.[18–20] One might thus expect that also for x-ray wavelengths, the spectral line shape of circular dichroism and magnetic Bragg reflections should be crucially influenced by the crystal symmetry.

To be able to present the results in a consistent picture, we first introduce a symmetry analysis of the magnetization direction dependence of the conductivity tensor or scattering tensor. This allows us to define a few linear independent spectra that describe the entire optical response of a system independent of the magnetization direction. These spectra we will call the fundamental spectra in line with the nomenclature as used by van der Laan and Arenholz.[21] Within this paper, we use symmetry labels according to nonmagnetic point groups. This represents the nonmagnetic part of the Hamiltonian. The Hamiltonian will furthermore contain a symmetry breaking sublattice magnetization in an arbitrary direction, given by $\boldsymbol{m} \equiv [m_x, m_y, m_z]$.[22] The full local point group belongs to a magnetic point group and is in general very low due to the arbitrarily orientated magnetization direction. The tensor formalism used is, in principle, valid for any type of magneto-optical experiment and closely related, though not entirely equivalent, to methods described in previous publications.[1–12,14–20] A relation between the scattering tensor on a basis of linear polarized light and a coupled multipole expansion of the polarization vectors can be found in the Appendix. The formalism can be used for the description of the crystal orientation dependence of the Kerr angle in the infrared regime on CrO_2,[19] x-ray vectorial magnetometry as used on thin films to determine the local magnetic domains,[23,24] or the magnetic Bragg diffraction of the cuprates at 930–950 eV.[25]

The first section presents a general derivation of the scattering tensor or conductivity tensor as a function of magnetization direction for several different point-group symmetries. We will express the scattering tensor as a 3×3 tensor on the basis of linear polarized light. In the Appendix, we will relate this notation to the use of coupled spherical tensors often used in the x-ray wavelength. In the second section, we will show how these tensors can be rewritten to simple dot products relating the scattered intensity to the polarization of the incoming and outgoing light in the same way as previously presented[1] in spherical symmetry. The third section is reserved for calculations of the fundamental spectra of several example materials in cubic point-group symmetry (the symmetry relates to the nonmagnetic point group the system would poses if no local magnetic moments were present). The numerical calculations are done with the use of crystal-field theory, which is particularly valid for the Transition metal $L_{2,3}$ edge of Mott-Hubbard insulators, such as cuperates, nickelates, manganates or other transition metal oxides, fluorides, chlorides, etc.[26–28] The fourth section presents results in tetragonal symmetry. Within the conclusions, we will discuss when deviation from spherical symmetry becomes visible in experiment and how the magnetization direction can be deduced from resonant x-ray diffraction experiments.

I. SCATTERING TENSOR OF SYSTEMS WITH ARBITRARY MAGNETIZATION DIRECTION

The general scattering tensor of a system of triclinic symmetry and an arbitrary magnetization is given by

$$F(\omega) = \begin{pmatrix} F_{xx}(\omega) & F_{yx}(\omega) & F_{zx}(\omega) \\ F_{xy}(\omega) & F_{yy}(\omega) & F_{zy}(\omega) \\ F_{xz}(\omega) & F_{yz}(\omega) & F_{zz}(\omega) \end{pmatrix} \tag{1}$$

which defines a nonsymmetric, non-Hermitian, complex tensor. Naturally this tensor can be diagonalized to give a complex basis defining the principal axes and a diagonal tensor. In general the principal axes will be ω dependent.[29–31] Even in high symmetries there will already be a strong ω dependence on the principal axes when a magnetization in an arbitrary direction is introduced.[32] It is therefore often more intuitive to stay in a Cartesian basis for the scattering tensor, with x, y, and z aligned along high-symmetry crystal axes.

Based on general symmetry arguments, the scattering tensor simplifies. We label the local point-group symmetry according to nonmagnetic point groups, whereby we take Γ to be the set of symmetry operations of this nonmagnetic point group. In the magnetically ordered phase there is an additional local magnetization. In the case that the local moment direction does not coincide with one of the high-symmetry axes of the nonmagnetic point group, only the identity operation is left of the original symmetry operations as all other symmetry operations will rotate the local moment. One can define a new set of symmetry operations Γ' that rotates first the entire system and then the local moment, i.e., the spin and orbital momentum, back. This would be the same as rotating the system but not the local moment.

In order to define symmetry operations that rotate the system but not the local moment, the scattering tensor needs to be written as a product of a function that is independent of the direction of the local moment but depends on ω and the polarization and a function that depends purely on the direction of the local moment. This can be done by expanding each element of the scattering tensor on spherical harmonics in the coordinates of the local moment,

$$F(\theta,\phi) = \sum_{k=0}^{\infty} \sum_{m=-k}^{k} \begin{pmatrix} F_{xx}^{km} & F_{yx}^{km} & F_{zx}^{km} \\ F_{xy}^{km} & F_{yy}^{km} & F_{zy}^{km} \\ F_{xz}^{km} & F_{yz}^{km} & F_{zz}^{km} \end{pmatrix} Y_{km}(\theta,\phi). \tag{2}$$

θ and ϕ define the direction of the local moment $[m_x = |\boldsymbol{m}|\cos(\phi)\sin(\theta)$, $m_y = |\boldsymbol{m}|\sin(\phi)\sin(\theta)$, and $m_z = |\boldsymbol{m}|\cos(\theta)]$, $Y_{k,m}$ is a spherical harmonic function and $F_{i,j}$ is the (i,j) component of the scattering tensor on a basis of linear polarized light in the coordinate system of the crystal $(\varepsilon_i, \varepsilon_j \in \{\varepsilon_x, \varepsilon_y, \varepsilon_z\})$. Note that both the local magnetization direction as well as the polarization are expressed in the same Cartesian coordinate system.

Natural dichroism effects due to any crystal symmetry are included in this formalism.[29–31] They are part of the expan-

sion coefficients with $k=0$. Any expansion with $k\neq 0$ becomes zero when averaged over all different magnetization directions. At the transition metal $L_{2,3}$ edge the natural linear dichroism for orbital ordered systems can become 100% in the cuprates but even if there is no orbital order in the ground state there can already be a substantial dichroism due to tetragonal crystal fields as shown, for example, in thin films of NiO.[33] Natural and magnetic dichroic effects can be of the same order of magnitude.

Finding the symmetry allowed components of the scattering tensor implies going through all symmetry operations possible and solving the equation $\Gamma' F = F$. This will lead to a set of allowed values for the expansion coefficients. For example, a $C_4'^z$ operation acting on $F(\theta,\phi)$, i.e., rotating the system but not rotating the magnetization direction, would give

$$C_4'^z F(\theta,\phi) = \sum_{k=0}^{\infty}\sum_{m=-k}^{k} \begin{pmatrix} F_{yy}^{km} & -F_{xy}^{km} & F_{zy}^{km} \\ -F_{yx}^{km} & F_{xx}^{km} & -F_{zx}^{km} \\ F_{yz}^{km} & -F_{xz}^{km} & F_{zz}^{km} \end{pmatrix} \times Y_{km}\left(\theta,\phi-\frac{1}{2}\pi\right) \tag{3}$$

which leads to sets of equations of the form $\Sigma_{k=0}^{\infty}\Sigma_{m=-k}^{k} F_{yx}^{km} Y_{km}(\theta,\phi) = -\Sigma_{k=0}^{\infty}\Sigma_{m=-k}^{k} F_{xy}^{km} Y_{km}(\theta,\phi-1/2\pi)$, which have to be solved.

Let us first discuss spherical symmetry. In spherical symmetry there should be no ϕ dependence and only terms with $m=0$ remain. Furthermore the infinite sum truncates at $k=2$ due to the triangular equations. This leaves only the expansion coefficients proportional to Y_{00}, Y_{10}, and Y_{20}. For a local moment in the z direction ($\hat{\boldsymbol{m}}=[001]$) one gets the known result,

$$F_{[001]} = \begin{pmatrix} F^{(0)} - \frac{1}{3}F^{(2)} & -F^{(1)} & 0 \\ F^{(1)} & F^{(0)} - \frac{1}{3}F^{(2)} & 0 \\ 0 & 0 & F^{(0)} + \frac{2}{3}F^{(2)} \end{pmatrix} \tag{4}$$

and for a local moment in the ($x \equiv m_x/|\boldsymbol{m}|, y \equiv m_y/|\boldsymbol{m}|, z \equiv m_z/|\boldsymbol{m}|$) direction,

$$F_{[xyz]} = \begin{pmatrix} F^{(0)} + \left(x^2 - \frac{1}{3}\right)F^{(2)} & -(z)F^{(1)} + (xy)F^{(2)} & (y)F^{(1)} + (xz)F^{(2)} \\ (z)F^{(1)} + (xy)F^{(2)} & F^{(0)} + \left(y^2 - \frac{1}{3}\right)F^{(2)} & -(x)F^{(1)} + (yz)F^{(2)} \\ -(y)F^{(1)} + (xz)F^{(2)} & (x)F^{(1)} + (yz)F^{(2)} & F^{(0)} + \left(z^2 - \frac{1}{3}\right)F^{(2)} \end{pmatrix}. \tag{5}$$

The result for a local moment in an arbitrary direction could also be obtained from the tensor of the local moment in the z direction by rotating the scattering tensor,

$$R = \begin{pmatrix} \cos(\phi) & -\sin(\phi) & 0 \\ \sin(\phi) & \cos(\phi) & 0 \\ 0 & 0 & 1 \end{pmatrix} \cdot \begin{pmatrix} \cos(\theta) & 0 & \sin(\theta) \\ 0 & 1 & 0 \\ -\sin(\theta) & 0 & \cos(\theta) \end{pmatrix} \tag{6}$$

then

$$F_{[xyz]} = R F_{[001]} R^T. \tag{7}$$

$F^{(1)}$ is related to the gyromagnetic vector by $\hat{\boldsymbol{m}} F^{(1)}/\omega \propto \imath \boldsymbol{g}$ and describes the magnetic circular dichroism or the Faraday effect. The $F^{(2)}$ components describe the magnetic linear dichroism. The magneto-optical Kerr Effect is given by both the $F^{(1)}$ and $F^{(2)}$ spectra depending on the experimental geometry.

In symmetries lower than spherical the expansion of the spin direction in spherical harmonics does not truncate at finite k. This has often been neglected previously but it becomes quite clear if one realizes that angular momentum of the electrons only is not a conserved quantum number in real crystals. Elements such as $F^{(3)}$, $F^{(4)}$, etc., are allowed by symmetry. There is thus, in principle, an infinite number of linear independent fundamental spectra. Not all of them are important and most of them will be very small. Below we will discus the higher-order expansions in more detail and give several numerical examples for realistic parameters. Furthermore, as previously discussed by Carra and Thole[10] the fundamental spectra of order k will branch according to their symmetry representations in the corresponding point group.

In cubic symmetry (O_h) the scattering tensor becomes ($C_4 \| \langle 001 \rangle$),

$$F_{[xyz]}=\begin{pmatrix} F^{(0)}_{a_{1g}}+\left(x^2-\frac{1}{3}\right)F^{(2)}_{e_g} & -zF^{(1)}_{t_{1u}}-z\left(z^2-\frac{3}{5}\right)F^{(3)}_{t_{1u}}+xyF^{(2)}_{t_{2g}} & yF^{(1)}_{t_{1u}}+y\left(y^2-\frac{3}{5}\right)F^{(3)}_{t_{1u}}+xzF^{(2)}_{t_{2g}} \\ zF^{(1)}_{t_{1u}}+z\left(z^2-\frac{3}{5}\right)F^{(3)}_{t_{1u}}+xyF^{(2)}_{t_{2g}} & F^{(0)}_{a_{1g}}+\left(y^2-\frac{1}{3}\right)F^{(2)}_{e_g} & -xF^{(1)}_{t_{1u}}-x\left(x^2-\frac{3}{5}\right)F^{(3)}_{t_{1u}}+yzF^{(2)}_{t_{2g}} \\ -yF^{(1)}_{t_{1u}}-y\left(y^2-\frac{3}{5}\right)F^{(3)}_{t_{1u}}+xzF^{(2)}_{t_{2g}} & xF^{(1)}_{t_{1u}}+x\left(x^2-\frac{3}{5}\right)F^{(3)}_{t_{1u}}+yzF^{(2)}_{t_{2g}} & F^{(0)}_{a_{1g}}+\left(z^2-\frac{1}{3}\right)F^{(2)}_{e_g} \end{pmatrix} \quad (8)$$

whereby the expansion series can be continued by summing for the diagonals the a_{1g} and e_g cubic harmonics of order k multiplied by a fundamental spectrum and for the off diagonal components the t_{1u} and t_{2g} cubic harmonics.

The important change between cubic and spherical symmetry is that $F^{(2)}$ becomes different ($F^{(2)}_{t_{2g}}$ or $F^{(2)}_{e_g}$) for diagonal and off diagonal elements in F. $F^{(2)}_{e_g}$ defines the magnetic linear dichroic spectrum one measures if the sample is magnetized along a C_4 direction whereas $F^{(2)}_{t_{2g}}$ defines the magnetic linear dichroic spectrum one measures if the sample is magnetized along a C_3 direction. For very small deviations from spherical symmetry $F^{(2)}_{t_{2g}}$ must be roughly equal to $F^{(2)}_{e_g}$, however as we will show below by several numerical examples one finds for real systems that $F^{(2)}_{e_g}$ and $F^{(2)}_{t_{2g}}$ are very different. On top of that one finds that for realistic parameters and large local moments the contribution of $F^{(3)}_{t_{1u}}$ cannot be neglected.

In tetragonal symmetry (D_{4h}) the scattering tensor becomes ($C_4 \| [001]$, $C_2 \| \langle 100 \rangle$),

$$F_{[xyz]}=\begin{pmatrix} F^{(0)}_{a^B_{1g}}+\frac{1}{2}(x^2-y^2)F^{(2)}_{b_{1g}}-\frac{1}{2}\left(z^2-\frac{1}{3}\right)F^{(2)}_{a^B_{1g}} & -zF^{(1)}_{a_{2u}}-z\left(z^2-\frac{3}{5}\right)F^{(3)}_{a_{2u}}+xyF^{(2)}_{b_{2g}} & yF^{(1)}_{e_u}+y\left(y^2-\frac{3}{5}\right)F^{(3)}_{e_u}+xzF^{(2)}_{e_g} \\ zF^{(1)}_{a_{2u}}+z\left(z^2-\frac{3}{5}\right)F^{(3)}_{a_{2u}}+xyF^{(2)}_{b_{2g}} & F^{(0)}_{a^B_{1g}}-\frac{1}{2}(x^2-y^2)F^{(2)}_{b_{1g}}-\frac{1}{2}\left(z^2-\frac{1}{3}\right)F^{(2)}_{a^B_{1g}} & -xF^{(1)}_{e_u}-x\left(x^2-\frac{3}{5}\right)F^{(3)}_{e_u}+yzF^{(2)}_{e_g} \\ -yF^{(1)}_{e_u}-y\left(y^2-\frac{3}{5}\right)F^{(3)}_{e_u}+xzF^{(2)}_{e_g} & xF^{(1)}_{e_u}+x\left(x^2-\frac{3}{5}\right)F^{(3)}_{e_u}+yzF^{(2)}_{e_g} & F^{(0)}_{a^A_{1g}}+\left(z^2-\frac{1}{3}\right)F^{(2)}_{a^A_{1g}} \end{pmatrix}. \quad (9)$$

The difference between $F^{(0)}_{a^A_{1g}}$ and $F^{(0)}_{a^B_{1g}}$ defines the natural linear dichroic spectra, also present in a paramagnetic sample.

There are five fundamental spectra up to order $k=2$ that describe the magnetic linear dichroism. Let us give examples how to obtain each one of these spectra. Placing the polarization into the z direction, the dichroism resulting from changing the magnetization direction from x to z is described by $F^{(2)}_{a^A_{1g}}$. When the polarization is along $[110]$ and the magnetization changes from x to z, $F^{(2)}_{a^B_{1g}}$ describes the magnetic linear dichroism. Placing the polarization along x, changing the magnetization from x to y will result in a magnetic linear dichroism determined by $F^{(2)}_{b_{1g}}$. There are two off-diagonal elements ($F^{(2)}_{b_{2g}}$ and $F^{(2)}_{e_g}$) that define the dichroism when the magnetization is in the $[111]$ direction: $F^{(2)}_{b_{2g}}$ for the dichroism between polarizations along $[110]$ and $[1\bar{1}0]$ and $F^{(2)}_{e_g}$ for polarizations along $[101]$ and $[10\bar{1}]$.

The isotropic spectrum, i.e., the spectrum measured on a powdered sample, is given by the trace of the conductivity tensor. The isotropic spectrum on a single crystal is measured by averaging three orthogonal polarization directions. For magnetic systems in cubic symmetry the trace is independent of the magnetization direction. The isotropic spectrum of a paramagnet is thus equal to the isotropic spectrum of the magnetically ordered system. It is interesting to note that the trace of the conductivity tensor in D_{4h} symmetry becomes dependent on the magnetization direction. This is due to the $F^{(2)}_{e_g}$ spectrum in cubic symmetry that branches to an $F^{(2)}_{a^A_{1g}}$ spectrum for z polarization and to an $F^{(2)}_{a^B_{1g}}$ and $F^{(2)}_{b_{1g}}$ spectrum for x or y polarization. This finding does not contradict that the spectrum of a paramagnet only depends on $k=0$ components. It is also valid that the spectrum of a multidomain sample averaged over all possible spin directions such that the final magnetic symmetry is at least cubic equals the spectrum of a paramagnet. The dependence of the trace of the conductivity tensor on the spin direction might therefore come as a surprise. However it is allowed by symmetry, which can be understood with an example. For a $S=1$ system one has three low-energy eigenstates, $S_z=1$, 0, or -1. With these three eigenstates any spin direction can be created.

Within cubic symmetry these three states still belong to the same irreducible representation (t_1) and rotating the spin therefore does not change the symmetry of the ground state. In tetragonal symmetry the $S_z=\pm 1$ states however have a different symmetry (e) from the $S_z=0$ state (a_2). Rotating the spin direction therefore changes the symmetry of the ground state and thus might change the x-ray absorption spectroscopy (XAS) spectra. Naively one might expect that this is unimportant as these states with different S_z will be degenerate as long as spin-orbit coupling for the d shell is neglected in the initial state. When spin-orbit coupling is included one might still expect that the splitting will be smaller than the magnetic field applied or the internal exchange fields present in the sample. But formally the ground-state symmetry changes depending on the magnetization direction and therefore the isotropic spectra (the trace of the conductivity tensor) might have a different line shape depending on having an e ($S_z=\pm 1$) or a_2 ($S_z=0$) ground state. The size of these effects will be shown below by numerical calculations.

In tetragonal symmetry the antisymmetric part of order $k=1$ cannot be represented by a single spectrum. The circular dichroic spectrum will be different for a magnetization direction parallel or perpendicular to the C_4 axes. In scattering experiments this fundamental spectrum determines the line shape of the first-order Bragg reflection of an antiferromagnetically ordered crystal. It will therefore have a large impact on the interpretation of scattering data.

In orthorhombic symmetry (D_{2h}) the scattering tensor becomes ($C_2 \| \langle 001 \rangle$)

$$F_{[xyz]} = \begin{pmatrix} F^{(0)}_{a^{xx}_g} + \left(x^2 - \frac{1}{3}\right)F^{(2)}_{a^{xxA}_g} + (y^2 - z^2)F^{(2)}_{a^{xxB}_g} & -zF^{(1)}_{b_{1u}} - z\left(z^2 - \frac{3}{5}\right)F^{(3)}_{b_{1u}} + xyF^{(2)}_{b_{1g}} & yF^{(1)}_{b_{2u}} + y\left(y^2 - \frac{3}{5}\right)F^{(3)}_{b_{2u}} + xzF^{(2)}_{b_{2g}} \\ zF^{(1)}_{b_{1u}} + z\left(z^2 - \frac{3}{5}\right)F^{(3)}_{b_{1u}} + xyF^{(2)}_{b_{1g}} & F^{(0)}_{a^{yy}_g} + \left(y^2 - \frac{1}{3}\right)F^{(2)}_{a^{yyA}_g} + (z^2 - x^2)F^{(2)}_{a^{yyB}_g} & -xF^{(1)}_{b_{3u}} - x\left(x^2 - \frac{3}{5}\right)F^{(3)}_{b_{3u}} + yzF^{(2)}_{b_{3g}} \\ -yF^{(1)}_{b_{2u}} - y\left(y^2 - \frac{3}{5}\right)F^{(3)}_{b_{2u}} + xzF^{(2)}_{b_{2g}} & xF^{(1)}_{b_{3u}} + x\left(x^2 - \frac{3}{5}\right)F^{(3)}_{b_{3u}} + yzF^{(2)}_{b_{3g}} & F^{(0)}_{a^{zz}_g} + \left(z^2 - \frac{1}{3}\right)F^{(2)}_{a^{zzA}_g} + (x^2 - y^2)F^{(2)}_{a^{zzB}_g} \end{pmatrix}. \tag{10}$$

II. POLARIZATION DEPENDENCE OF SCATTERED INTENSITY

The scattering tensor cannot be measured directly. Absorption, reflection, scattering, or diffraction experiments measure different parts or combinations of the tensor. An absorption measurement probes the imaginary part of σ,

$$I_{abs} = -\Im\left[\sum_i \boldsymbol{\varepsilon}^* \cdot \sigma_i \cdot \boldsymbol{\varepsilon}\right] \tag{11}$$

with $\boldsymbol{\varepsilon}$ the polarization of the light and σ_i the conductivity tensor of atom i. The sum is over all atoms in the sample (neglecting self-absorption effects) and $\sigma_i \propto F_i/\omega$. The real part can then be obtained from a Kramers-Kronig transformation.

In a reflection, scattering or diffraction experiment one measures

$$I_{scat} = \left|\sum_i e^{\imath(\boldsymbol{k}_{in}-\boldsymbol{k}_{out})\cdot \boldsymbol{r}_i} \boldsymbol{\varepsilon}^*_{out} \cdot F_i \cdot \boldsymbol{\varepsilon}_{in}\right|^2 \tag{12}$$

with $\boldsymbol{\varepsilon}_{in(out)}$ the polarization of the incoming (outgoing) light, $\boldsymbol{k}_{in(out)}$ the wave vector of the incoming (outgoing) light, $\boldsymbol{r}_i$ the position of atom i, F_i the scattering tensor of atom i and the sum over all atoms in the sample (neglecting self-absorption effects).

The polarization cannot be chosen arbitrarily in a diffraction experiment, as the $\boldsymbol{k}$ vectors of the light must fulfill the Bragg condition. The polarization has to be perpendicular to $\boldsymbol{k}$, leaving two options for the polarization: $\boldsymbol{\varepsilon}$ can be in the scattering plane ($\boldsymbol{\pi}$ polarization) or $\boldsymbol{\varepsilon}$ can be perpendicular to the scattering plane ($\boldsymbol{\sigma}$ polarization). Theoretically it is easier to work in Cartesian coordinates and describe the material properties independent of the measurement geometry. We express the magnetization direction, the Poynting vectors of the light as well as the polarization in the same coordinate system. It is thus needed to find an easy expression of $\boldsymbol{\sigma}$ and $\boldsymbol{\pi}$ polarization in this coordinate frame. We will take that $\boldsymbol{a}$, $\boldsymbol{b}$, and $\boldsymbol{c}$, (the lattice vectors) and the scattering vector ($\boldsymbol{k}_{out} - \boldsymbol{k}_{in} = \boldsymbol{q} \equiv [q_x, q_y, q_z]$) are known in real-space Cartesian coordinates.[22] In order to define the scattering plane we will need a second vector that might arbitrarily be chosen but must be perpendicular to $\boldsymbol{q}$, which we will call $\boldsymbol{q}_\perp$. Then ϕ will be the azimuthal angle, defined as the angle between $\boldsymbol{q}_\perp$ and the scattering plane. The angle between $\boldsymbol{q}$ and $\boldsymbol{k}_{in}$ will be written as θ'. (The angle between $\boldsymbol{q}$ and $\boldsymbol{k}_{out}$ then is $\pi - \theta'$.) This leads to the following definitions for the $\boldsymbol{k}$ vectors of the light and $\boldsymbol{\sigma}$ and $\boldsymbol{\pi}$ polarization in Cartesian coordinates;

$$\boldsymbol{k}_{in} \| \sin(\theta')[\cos(\phi)\hat{\boldsymbol{q}}_\perp + \sin(\phi)(\hat{\boldsymbol{q}}_\perp \times \hat{\boldsymbol{q}})] + \cos(\theta')\hat{\boldsymbol{q}},$$

$$\boldsymbol{k}_{out} \| \sin(\theta')[\cos(\phi)\hat{\boldsymbol{q}}_\perp + \sin(\phi)(\hat{\boldsymbol{q}}_\perp \times \hat{\boldsymbol{q}})] - \cos(\theta')\hat{\boldsymbol{q}},$$

$$\boldsymbol{\sigma} = (\hat{\boldsymbol{k}}_{in} \times \hat{\boldsymbol{k}}_{out})/\sin(2\theta'),$$

$$\boldsymbol{\pi}_{in} = (\hat{\boldsymbol{k}}_{in} \times \boldsymbol{\sigma}),$$

$$\boldsymbol{\pi}_{out} = (\hat{\boldsymbol{k}}_{out} \times \boldsymbol{\sigma}). \tag{13}$$

The polarization of the incoming (outgoing) light can be written in Cartesian coordinates as $\boldsymbol{\varepsilon}_{in(out)} = \alpha\boldsymbol{\sigma} + \beta\boldsymbol{\pi}_{in(out)}$, with α and β complex numbers such that $\alpha^*\alpha + \beta^*\beta = 1$.

For a given azimuth angle ϕ (and $\boldsymbol{k}_{in}$, $\boldsymbol{k}_{out}$, θ, and $\boldsymbol{q}$) one can measure four independent spectra for the different possible π and σ polarization for the incoming and outgoing light. These spectra would be $|F_{\sigma\sigma}|^2$, $|F_{\sigma\pi}|^2$, $|F_{\pi\sigma}|^2$, and $|F_{\pi\pi}|^2$. As it is often experimentally easier to change the incoming polarization and not use a polarization analyzer of the outgoing light one might choose to measure four linear independent spectra in a different fashion. One can use incoming σ or π linear polarized light, 45° linear-polarized rotated light $(\sigma+\pi)$ and circular $(\sigma+\imath\pi)$ polarized light. These four spectra are also linear independent and, in principle, fully determine the scattering tensor on a basis of σ and π polarization. It might however not be trivial to obtain the scattering tensor on a basis of σ and π polarized light from the measurements without an outgoing polarization filter.

For a given polarization the scattering tensor can be obtained in terms of dot and cross products of the polarization and a unit vector in the local moment direction $(\hat{\boldsymbol{m}})$. Hannon and Blume *et al.*[1] came to the following formula in spherical symmetry:

$$F_{\boldsymbol{\varepsilon}_{in}\boldsymbol{\varepsilon}_{out}} = F^{(0)}(\boldsymbol{\varepsilon}_{in}\cdot\boldsymbol{\varepsilon}^*_{out}) + F^{(1)}(\boldsymbol{\varepsilon}_{in}\times\boldsymbol{\varepsilon}^*_{out}\cdot\hat{\boldsymbol{m}}) + F^{(2)}\left[(\boldsymbol{\varepsilon}^*_{out}\cdot\hat{\boldsymbol{m}})(\boldsymbol{\varepsilon}_{in}\cdot\hat{\boldsymbol{m}}) - \frac{1}{3}(\boldsymbol{\varepsilon}_{in}\cdot\boldsymbol{\varepsilon}^*_{out})\right] \tag{14}$$

which can be derived by dotting the scattering tensor in spherical symmetry for arbitrary spin direction with $\boldsymbol{\varepsilon}^*_{out}$ and $\boldsymbol{\varepsilon}_{in}$ and some algebra.

In cubic (O_h) symmetry $F_{\boldsymbol{\varepsilon}_{in}\boldsymbol{\varepsilon}_{out}}$ becomes

$$\begin{aligned}
&= F^{(0)}_{a_{1g}}(\boldsymbol{\varepsilon}_{in}\cdot\boldsymbol{\varepsilon}^*_{out}) + F^{(1)}_{t_{1u}}(\boldsymbol{\varepsilon}_{in}\times\boldsymbol{\varepsilon}^*_{out}\cdot\hat{\boldsymbol{m}}) + F^{(2)}_{t_{2g}}[(\boldsymbol{\varepsilon}^*_{out}\cdot\hat{\boldsymbol{m}})(\boldsymbol{\varepsilon}_{in}\cdot\hat{\boldsymbol{m}}) - (\boldsymbol{\varepsilon}^*_{out}*\hat{\boldsymbol{m}})\cdot(\boldsymbol{\varepsilon}_{in}*\hat{\boldsymbol{m}})] \\
&\quad + F^{(2)}_{e_g}\left[(\boldsymbol{\varepsilon}^*_{out}*\hat{\boldsymbol{m}})\cdot(\boldsymbol{\varepsilon}_{in}*\hat{\boldsymbol{m}}) - \frac{1}{3}(\boldsymbol{\varepsilon}_{in}\cdot\boldsymbol{\varepsilon}^*_{out})\right] + F^{(3)}_{t_{1u}}\left\{\boldsymbol{\varepsilon}_{in}\times\boldsymbol{\varepsilon}^*_{out}\cdot\left[\hat{\boldsymbol{m}}*\left(\hat{\boldsymbol{m}}*\hat{\boldsymbol{m}} - \frac{3}{5}\right)\right]\right\}
\end{aligned} \tag{15}$$

with "×" the standard vector cross product, "·" the vector dot product and "*" stands for vector multiplication per index $(\boldsymbol{a} = \boldsymbol{b}*\boldsymbol{c} \Leftrightarrow a_i = b_i c_i \,\forall\, i)$.

In tetragonal symmetry (D_{4h}) one obtains

$$\begin{aligned}
&= F^{(0)}_{a^B_{1g}}(\boldsymbol{\varepsilon}_{in_{xy}}\cdot\boldsymbol{\varepsilon}^*_{out_{xy}}) + F^{(0)}_{a^A_{1g}}(\boldsymbol{\varepsilon}_{in_z}\cdot\boldsymbol{\varepsilon}^*_{out_z}) + F^{(1)}_{e_u}(\boldsymbol{\varepsilon}_{in}\times\boldsymbol{\varepsilon}^*_{out}\cdot\hat{\boldsymbol{m}}_{xy}) + F^{(1)}_{a_{2u}}(\boldsymbol{\varepsilon}_{in}\times\boldsymbol{\varepsilon}^*_{out}\cdot\hat{\boldsymbol{m}}_z) \\
&\quad + F^{(2)}_{e_g}[(\boldsymbol{\varepsilon}^*_{out}\cdot\hat{\boldsymbol{m}}_{xy})(\boldsymbol{\varepsilon}_{in}\cdot\hat{\boldsymbol{m}}_z) + (\boldsymbol{\varepsilon}^*_{out}\cdot\hat{\boldsymbol{m}}_z)(\boldsymbol{\varepsilon}_{in}\cdot\hat{\boldsymbol{m}}_{xy})] + F^{(2)}_{b_{2g}}[(\boldsymbol{\varepsilon}^*_{out}\cdot\hat{\boldsymbol{m}}_x)(\boldsymbol{\varepsilon}_{in}\cdot\hat{\boldsymbol{m}}_y) + (\boldsymbol{\varepsilon}^*_{out}\cdot\hat{\boldsymbol{m}}_y)(\boldsymbol{\varepsilon}_{in}\cdot\hat{\boldsymbol{m}}_x)] \\
&\quad + F^{(2)}_{b_{1g}}\frac{1}{2}(m_x^2 - m_y^2)(\boldsymbol{\varepsilon}_{in_x}\cdot\boldsymbol{\varepsilon}^*_{out_x} - \boldsymbol{\varepsilon}_{in_y}\cdot\boldsymbol{\varepsilon}^*_{out_y}) + F^{(2)}_{a^A_{1g}}\left(m_z^2 - \frac{1}{3}\right)(\boldsymbol{\varepsilon}_{in_z}\cdot\boldsymbol{\varepsilon}^*_{out_z}) + F^{(2)}_{a^B_{1g}}\left(m_z^2 - \frac{1}{3}\right)(\boldsymbol{\varepsilon}_{in_{xy}}\cdot\boldsymbol{\varepsilon}^*_{out_{xy}}) \\
&\quad + F^{(3)}_{e_u}\left\{\boldsymbol{\varepsilon}_{in}\times\boldsymbol{\varepsilon}^*_{out}\cdot\left[\hat{\boldsymbol{m}}_{xy}*\left(\hat{\boldsymbol{m}}*\hat{\boldsymbol{m}} - \frac{3}{5}\right)\right]\right\} + F^{(3)}_{a_{2u}}\left\{\boldsymbol{\varepsilon}_{in}\times\boldsymbol{\varepsilon}^*_{out}\cdot\left[\hat{\boldsymbol{m}}_z*\left(\hat{\boldsymbol{m}}*\hat{\boldsymbol{m}} - \frac{3}{5}\right)\right]\right\}
\end{aligned} \tag{16}$$

with $\hat{\boldsymbol{m}}_z$ a vector with only the z component of $\hat{\boldsymbol{m}}$ nonzero, i.e., $[0,0,m_z/|\boldsymbol{m}|]$ and $\boldsymbol{\varepsilon}_{in_{xy}}$ a vector with only the x and y projection of $\boldsymbol{\varepsilon}_{in}$ nonzero, i.e., $\boldsymbol{\varepsilon}_{in_{xy}} = [\varepsilon_x, \varepsilon_y, 0]$. The orthorhombic (D_{2h}) relations are

$$\begin{aligned}
&= F^{(0)}_{a^{xx}_g}(\boldsymbol{\varepsilon}_{in_x}\cdot\boldsymbol{\varepsilon}^*_{out_x}) + F^{(0)}_{a^{yy}_g}(\boldsymbol{\varepsilon}_{in_y}\cdot\boldsymbol{\varepsilon}^*_{out_y}) + F^{(0)}_{a^{zz}_g}(\boldsymbol{\varepsilon}_{in_z}\cdot\boldsymbol{\varepsilon}^*_{out_z}) + F^{(1)}_{b_{1u}}(\boldsymbol{\varepsilon}_{in}\times\boldsymbol{\varepsilon}^*_{out}\cdot\hat{\boldsymbol{m}}_z) + F^{(1)}_{b_{2u}}(\boldsymbol{\varepsilon}_{in}\times\boldsymbol{\varepsilon}^*_{out}\cdot\hat{\boldsymbol{m}}_y) \\
&\quad + F^{(1)}_{b_{3u}}(\boldsymbol{\varepsilon}_{in}\times\boldsymbol{\varepsilon}^*_{out}\cdot\hat{\boldsymbol{m}}_x) + F^{(2)}_{b_{1g}}[(\boldsymbol{\varepsilon}^*_{out}\cdot\hat{\boldsymbol{m}}_x)(\boldsymbol{\varepsilon}_{in}\cdot\hat{\boldsymbol{m}}_y) + (\boldsymbol{\varepsilon}^*_{out}\cdot\hat{\boldsymbol{m}}_y)(\boldsymbol{\varepsilon}_{in}\cdot\hat{\boldsymbol{m}}_x)] \\
&\quad + F^{(2)}_{b_{2g}}[(\boldsymbol{\varepsilon}^*_{out}\cdot\hat{\boldsymbol{m}}_z)(\boldsymbol{\varepsilon}_{in}\cdot\hat{\boldsymbol{m}}_x) + (\boldsymbol{\varepsilon}^*_{out}\cdot\hat{\boldsymbol{m}}_x)(\boldsymbol{\varepsilon}_{in}\cdot\hat{\boldsymbol{m}}_z)] + F^{(2)}_{b_{3g}}[(\boldsymbol{\varepsilon}^*_{out}\cdot\hat{\boldsymbol{m}}_y)(\boldsymbol{\varepsilon}_{in}\cdot\hat{\boldsymbol{m}}_z) + (\boldsymbol{\varepsilon}^*_{out}\cdot\hat{\boldsymbol{m}}_z)(\boldsymbol{\varepsilon}_{in}\cdot\hat{\boldsymbol{m}}_y)] \\
&\quad + \left[F^{(2)}_{a^{xxA}_g}\left(m_z^2 - \frac{1}{3}\right) + F^{(2)}_{a^{xxB}_g}(m_x^2 - m_y^2)\right](\boldsymbol{\varepsilon}_{in_x}\cdot\boldsymbol{\varepsilon}^*_{out_x}) + \left[F^{(2)}_{a^{yyA}_g}\left(m_z^2 - \frac{1}{3}\right) + F^{(2)}_{a^{yyB}_g}(m_x^2 - m_y^2)\right](\boldsymbol{\varepsilon}_{in_y}\cdot\boldsymbol{\varepsilon}^*_{out_y}) \\
&\quad + \left[F^{(2)}_{a^{zzA}_g}\left(m_z^2 - \frac{1}{3}\right) + F^{(2)}_{a^{zzB}_g}(m_x^2 - m_y^2)\right](\boldsymbol{\varepsilon}_{in_z}\cdot\boldsymbol{\varepsilon}^*_{out_z}) + F^{(3)}_{b_{1u}}\left\{\boldsymbol{\varepsilon}_{in}\times\boldsymbol{\varepsilon}^*_{out}\cdot\left[\hat{\boldsymbol{m}}_z*\left(\hat{\boldsymbol{m}}*\hat{\boldsymbol{m}} - \frac{3}{5}\right)\right]\right\} \\
&\quad + F^{(3)}_{b_{2u}}\left\{\boldsymbol{\varepsilon}_{in}\times\boldsymbol{\varepsilon}^*_{out}\cdot\left[\hat{\boldsymbol{m}}_y*\left(\hat{\boldsymbol{m}}*\hat{\boldsymbol{m}} - \frac{3}{5}\right)\right]\right\} + F^{(3)}_{b_{3u}}\left\{\boldsymbol{\varepsilon}_{in}\times\boldsymbol{\varepsilon}^*_{out}\cdot\left[\hat{\boldsymbol{m}}_x*\left(\hat{\boldsymbol{m}}*\hat{\boldsymbol{m}} - \frac{3}{5}\right)\right]\right\}.
\end{aligned} \tag{17}$$

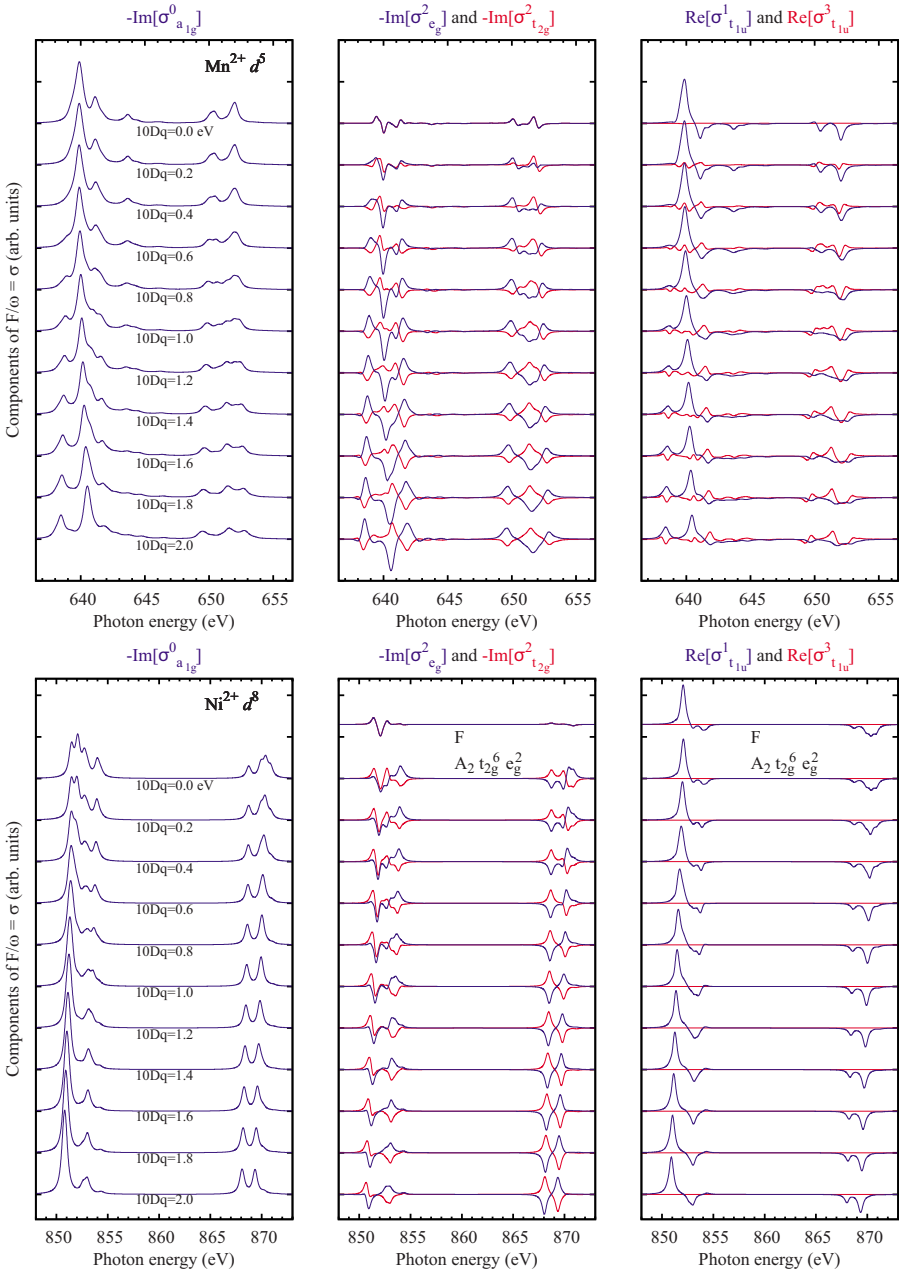

FIG. 1. (Color online) Scattering tensor of (top) Mn^{2+} and (bottom) Ni^{2+} as a function of the cubic crystal-field splitting $10Dq$. Left column shows the a_{1g} component, middle column the t_{2g} and e_g component and right column the t_{1u} component. All graphs are on the same intensity scale. For Ni^{2+} with $10Dq=0$ two graphs are included, once starting from a spherical ground state (F) and once starting from the cubic ground state (A_2). Calculations done on an ionic model without spin-orbit coupling on the d shell.

III. Mn^{2+} AND Ni^{2+} IN CUBIC SYMMETRY

The question that still has to be answered is whether the differences in intensity between spherical and lower symmetries are large enough to be observed. We therefore calculated a few examples at the transition metal $L_{2,3}$ edge using the multiplet crystal-field approach. The parameters for such calculations are well discussed in the literature,[27,34–36] and we adopted those values. The size of the crystal-field splitting between the t_{2g} and e_g orbitals, $10Dq$, varies from material to material, but several trends can be given. For the late transition metal 2+ oxides such as NiO or CoO one finds $10Dq \approx 1.0-1.5$ eV.[27,35,37–39] For 3+ late transition metal oxides such as $LaCoO_3$ the size of $10Dq$ is larger then for the 2+ compounds due to the smaller charge-transfer energy and enlarged covalency. For $LaCoO_3$ $10Dq$ is around $\approx 2.0-2.5$ eV.[40] For early transition metal oxides, which have slightly larger radial wave functions and no occupied antibonding e_g orbitals, one generally finds larger values of the crystal-field parameters.[27,35,36] For fluorides, which are less covalent, one finds slightly smaller crystal-field parameters.[34]

In order to show the evolution from spherical to cubic symmetry we first show the evolution of the fundamental spectra a function of the cubic crystal-field parameter $10Dq$. We also show an example of the magnetic resonant x-ray diffraction spectra at the Mn L_2 edge of an artificial $(MnO)_6NiO$ superlattice including all experimental geometries. For the calculation of the fundamental spectra as a function of $10Dq$ we did not include the $3d$ spin-orbit coupling nor covalency (crystal-field theory instead of ligand-field theory) in order to make the interpretation easier. While we did not include spin orbit coupling on the d shell the magnetization direction directly coincides with the spin di-

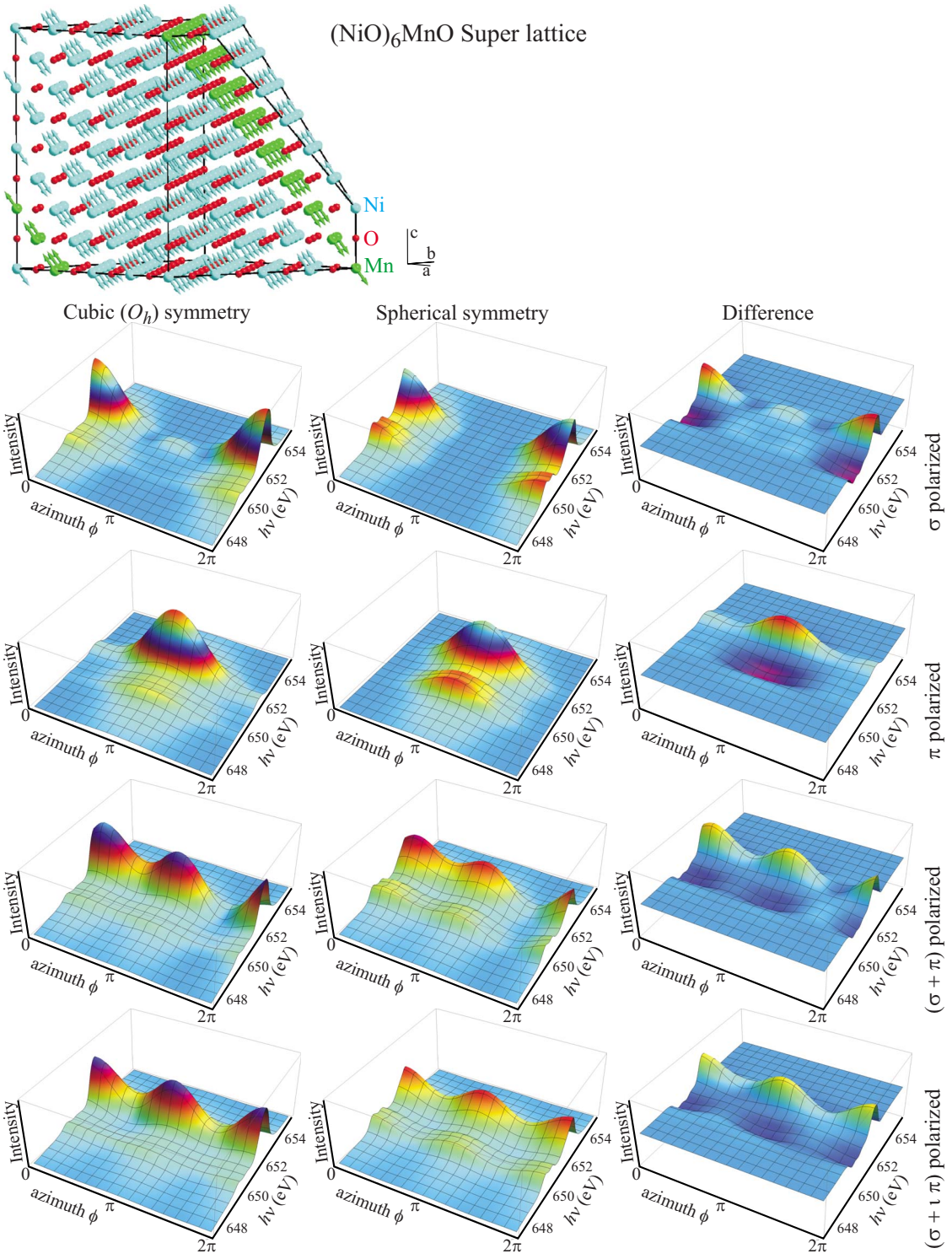

FIG. 2. (Color online) Top: an artificially created super lattice of six layers of NiO alternated by one layer of MnO stacked in the [111] cubic crystal direction. Bottom: RXD intensity of the first magnetic Bragg reflection as a function of the azimuthal angle ϕ and resonant energy. In the left column calculations are done for the scattering tensor in cubic symmetry. In the middle column spherical symmetry has been created by taking $F^{(1)}$ proportional to the average of F_{xy}, F_{zy} and F_{xz} as calculated in cubic symmetry. The calculations are done for incoming σ, π, linear 45° rotated ($\sigma+\pi$), and circular ($\sigma+\imath\pi$) polarized light.

rection. The spectra are calculated at 0 K and assume a full magnetization. The calculations have been done with the full multiplet ligand field theory program XTLS 8.3.[35] The fundamental spectra can be obtained by doing calculations for specific spin orientations. On top of those calculations a basic check has been made where the optical conductivity tensor has been calculated for many different magnetization directions. The result is expanded on spherical harmonics in co-

ordinates of the magnetization direction. Both methods gave the same results within the numerical accuracy of the calculations.

In the top panel of Fig. 1 we show the $L_{2,3}$ edge x-ray absorption spectra of Mn^{2+} as a function of the cubic splitting parametrized by $10Dq$. The top spectrum has $10Dq=0$ and is therefore in spherical symmetry. The ground state has always five electrons with parallel spin occupied and the ground-state wave function is independent of the crystal-field splitting. All changes in the spectra are due to final-state effects whereby the $2p$ core hole is excited into a t_{2g} or e_g electron and the energy difference between the two changes as a function of $10Dq$. The left panel shows $F^{(0)}_{a_{1g}}$, which is the isotropic spectrum and the spectrum of the paramagnetic phase. These spectra are the same as published earlier by de Groot *et al.*[34] The middle column shows $F^{(2)}_{e_g}$ and $F^{(2)}_{t_{2g}}$. These two spectra describe the magnetic linear dichroic effect. In spherical symmetry (top curve, $10Dq=0$) these two spectra are the same. However when a cubic distortion is present these two spectra become different. For a commensurate spin spiral one would expect a different resonant profile at the second order Bragg peak depending on the phase of the spiral with respect to the cubic crystal structure, i.e., a spiral with period $4z$ and the spins in the x, y, $-x$, $-y$ direction would show an $|F^{(2)}_{e_g}|^2$ like second-order resonance profile whereas a spiral at the same q vector but shifted in phase such that the spin directions are $x+y$, $-x+y$, $-x-y$, $x-y$ would show an $|F^{(2)}_{t_{2g}}|^2$ like second-order resonance profile. For x-ray absorption this has implications for the measured magnetic linear dichroism as explained previous by Arenholz and van der Laan *et al.*[14–16]

The right column of Fig. 1 shows the $F^{(1)}_{t_{1u}}$ and $F^{(3)}_{t_{1u}}$ spectra. In O_h symmetry the $k=1$ spectra branch to a single representation (a t_{1u}). Additionally angular momentum (k) is not a good quantum number in cubic symmetry and therefore the $F^{(3)}_{t_{1u}}$ spectra becomes nonzero. For spectroscopy this means a difference in the magnetic circular dichroism spectra for a system magnetized in the [001] direction where one measures $\Re[\sigma^1_{t_{1u}}+2/5\sigma^3_{t_{1u}}]$ and the [111] direction where the measured spectrum is $\Re[\sigma^1_{t_{1u}}-4/15\sigma^3_{t_{1u}}]$. Which has experimentally been observed on Mn doped GaAs crystals.[41] For resonant diffraction at an antiferromagnetic Bragg reflection this will lead to a different resonance profile depending if the spins are ordered in the [001] or [111] direction. It will also lead to a different azimuthal dependence of the scattered intensity at an antiferromagnetic Bragg reflection. For spins oriented in the $[11\bar{2}]$ direction ferromagnetically aligned in (111) planes, antiferromagnetically stacked in the [111] direction (as depicted in the top panel of Fig. 2) and a scattering geometry such that $\theta'=\pi/6$ one finds a scattered intensity proportional to $|F^{(3)}/(2\sqrt{6})\pm\sin(\phi)(10F^{(1)}-F^{(3)})/20|^2$ in the $\pi-\sigma$ ($\sigma-\pi$) scattering channel. For different spin alignments the ϕ-independent scattering due to the $F^{(1)}$ scattering tensor would be related to the projection of the spin on the $\boldsymbol{q}$ vector. Measurements at a single resonant energy could thus lead to incorrect determination of the spin direction. However $F^{(3)}$ has a different ω dependence than $F^{(1)}$ and this can be used to obtain the correct spin direction from such experiments.

The size of this effect on the measured intensity can be seen in Fig. 2 where resonant x-ray diffraction intensities for a $(NiO)_6MnO$ multilayer system have been calculated including the experimental geometry. The calculations are done for scattering at the first-order magnetic Bragg reflection at the Mn L_2 edge. The distance between two Mn layers is $\approx 7\times 2.4$ Å, which results in a scattering angle θ' as defined in Eq. (13) of $\theta'=73.5°$ at a photon energy of 650 eV. The vector $\boldsymbol{q}$ points in the [111] direction. The vector $\boldsymbol{q}_\perp$ has been chosen to be in the $[11\bar{2}]$ direction, which then defines the definitions of σ and π polarization as a function of the azimuthal angle ϕ [see Eq. (13)]. It is assumed that one scatters of a single magnetic domain as described above and depicted in the top panel of Fig. 2. The scattered intensity for different azimuth angles and resonant energies at the Mn L_2 edge can be seen in the bottom panels of Fig. 2. The left columns show the scattered intensity as calculated in O_h symmetry. The ligand-field parameters are the same as have been used in the literature before.[35] There is a distinct difference between incoming σ, π, polarized light, 45° linear-polarized rotated light ($\sigma+\pi$), and circular ($\sigma+\imath\pi$) polarized light as can be seen in the four different rows. The middle column shows the calculated spectra assuming spherical symmetry for the scattering tensor. Spherical symmetry has been created by averaging the calculated scattering tensor in cubic symmetry. In spherical symmetry the scattering cross section is given by a single function, namely $F^{(1)}$. This function has been taken to be the average of the calculated tensor elements $F^{(1)}=(\sqrt{6}/4)(F_{xy}+F_{yz}+F_{xz})$. The right column shows the difference between spherical and cubic symmetry. The intensity scale is the same for all graphs in a single row. One can see that on average there is a shift of diffracted intensity from the low to higher energy peak when going from spherical to cubic symmetry. This is not a general feature but depends on the specific geometry. One also finds that there are clearly visible changes in the angular dependence. For σ polarized light one finds in cubic symmetry a local maximum of the scattered intensity at $\phi=\pi$ whereas in spherical symmetry this maximum is not visible. Furthermore as one can see clearly in the graphs for π polarized light, there is a different azimuthal independent intensity in both cases. The differences can become around 40% of the intensity but the general line shape is not hugely changed, however for a system starting with a d^5 configuration and basically having a spherical ground state the differences are surprisingly large. This does not mean that all scattering data so far have to be reinterpreted. Whenever the spin orders in a high-symmetry direction ([001] or [111], for example) one would not see a difference between the calculations done in spherical symmetry or cubic symmetry. This becomes immediately clear if one considers the scattering tensor for such spin directions as given in Eq. (8) and compares this to the scattering tensor as found in spherical symmetry [Eq. (5)]. For most systems the spins do order in high-symmetry directions and thus, as long as the symmetry is high the formulas as derived in spherical symmetry, although not formally valid, still give correct answers. For MnO and NiO the spin orders in $\langle 11\bar{2}\rangle$ directions and thus the deviations between spherical and cubic symmetry become important.

The bottom panel of Fig. 1 shows the fundamental spectra, for Ni^{2+}. The major difference between a d^8 system (Ni^{2+}) and a d^5 system (Mn^{2+}) is that for a d^8 system the ground state is modified when a cubic crystal field is included. In spherical symmetry both the e_g and t_{2g} orbitals are equally occupied, in cubic symmetry this is not the case. When $10Dq=0$ and a spherical charge distribution is assumed for the initial state one finds that the $F^{(2)}_{e_g}$ and $F^{(2)}_{t_{2g}}$ spectra are equivalent (middle panel top curve labeled as F). If one however assumes a $t^6_{2g}e^2_g$ orbital occupation as one would find as a ground state in cubic symmetry one finds a large difference between the $F^{(2)}_{e_g}$ and $F^{(2)}_{t_{2g}}$ spectra (middle panel second curve from top labeled as A_2). It is important to note the difference between Mn^{2+} and Ni^{2+}. For a perturbation that does not lift the ground-state degeneracy the changes in spectra scale with the size of the distortion whereas for a perturbation that lifts the ground-state degeneracy there will be an immediate large effect on the spectral line shape as long as the distortion is bigger than temperature. The symmetry breaking is important for orbitally ordered systems. Above the ordering temperature, the system can be described by the scattering tensor in the higher symmetry. Although the distortions may be small in the orbitally ordered phase, breaking the ground-state symmetry will have an immediate effect on the spectra. Thus even small distortions can lead to relevant changes in the scattering tensor.

IV. Ni^{2+}, Mn^{3+}, AND Cu^{2+} IN TETRAGONAL SYMMETRY

In tetragonal symmetry the $F^{(0)}$ spectrum branches to $F^{(0)}_{a^A_{1g}}$ and $F^{(0)}_{a^B_{1g}}$, the $F^{(1)}$ spectrum branches to $F^{(1)}_{a_{2u}}$ and $F^{(1)}_{a_{eu}}$, and the $F^{(2)}$ spectrum branches to $F^{(2)}_{b_{2g}}$, $F^{(2)}_{e_g}$, $F^{(2)}_{b_{1g}}$, $F^{(2)}_{a^A_{1g}}$, and $F^{(2)}_{a^B_{1g}}$. To estimate the numerical differences between these spectra at the $L_{2,3}$ edge we again did crystal-field calculations. We did calculations for a variety of different crystal-field parameters. Experimental values can depend strongly on the material at hand. For strained thin films of CoO or NiO one can find tetragonal distortions of the size of 10–100 meV.[39,33] For early transition metal compounds similar distortions can give rise to substantial larger crystal-field splittings on the order of several 100 meV.[42,43] Much larger crystal-field splittings are found in systems with an open e_g subshell and for several layered cuprates structures an energy difference of $\approx 1-3$ eV between the $d_{x^2-y^2}$ and d_{z^2} hole has been found.[44]

The top panel of Fig. 3 shows the spectra for Ni^{2+} as a function of tetragonal distortion. In the middle we show cubic symmetry and toward the top (bottom) a tetragonal contraction (elongation). The Ni^{2+} ground state does not change as a function of tetragonal distortion and therefore the difference between spectra that branch from the same irreducible representation in cubic symmetry scale with the size of the tetragonal distortion. The left panel shows the natural linear dichroism in tetragonal distorted Ni^{2+} which has been discussed before.[33] Note that for large tetragonal distortions it can have a similar magnitude as the magnetic dichroism. The second panel from the left shows the magnetic linear dichroism that branches from the cubic e_g representation. Interestingly, *three* fundamental spectra represent the linear dichroism that branches from the e_g representation in cubic symmetry and for feasible distortions they are all different. The trace of the conductivity tensor, or the isotropic spectrum, is thus dependent on the magnetization direction and

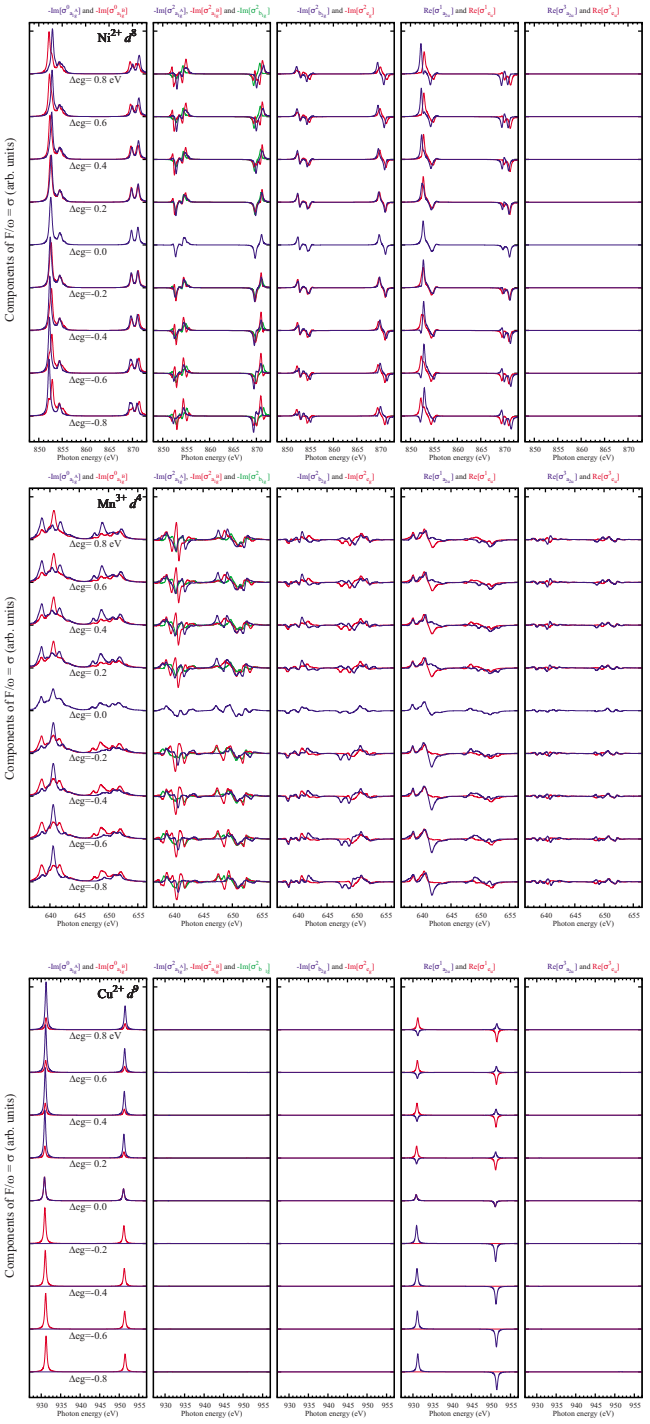

FIG. 3. (Color online) Fundamental spectra of the elastic scattering tensor for Ni^{2+} (top panel), Mn^{3+} (middle panel), and Cu^{3+} (bottom panel) as a function of tetragonal crystal-field splitting Δe_g defined as the energy difference between the d_{z^2} and $d_{x^2-y^2}$ orbital. ($\Delta t_{2g}=1/4\Delta e_g$). $\Delta e_g>0$ stands for a tetragonal contracted system, i.e., the d_{z^2} orbital higher in energy than the $d_{x^2-y^2}$ orbital.

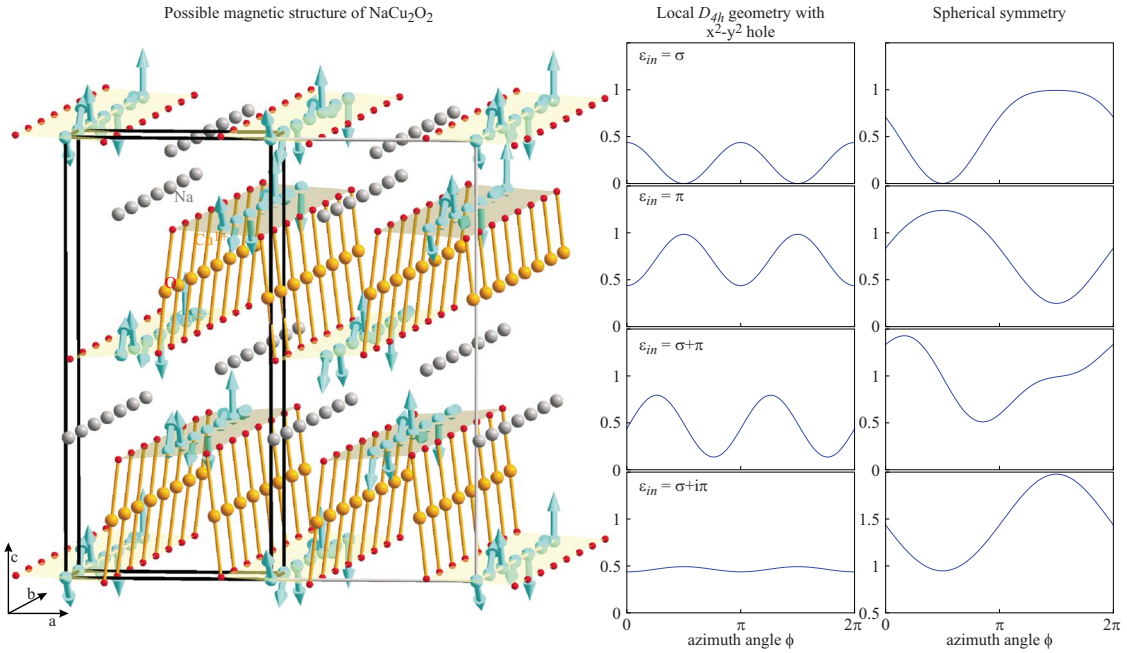

FIG. 4. (Color online) Left: crystal structure of $NaCu_2O_2$ including a possible local magnetization direction, which is used for the RXD calculations. Right: RXD calculations of the scattered intensity as a function of the azimuthal angle, for incoming σ, π, linear 45° rotated $(\sigma+\pi)$, and circular $(\sigma+\imath\pi)$ polarized light. Whereby the scattering tensor once has been assumed to have tetragonal symmetry and once has been assumed to have spherical symmetry.

the difference is large enough to be detectable. The isotropic spectrum in D_{4h} symmetry is given by $(1/3)(2F^{(0)}_{a^B_{1g}}+F^{(0)}_{a^A_{1g}}+(z^2-1/3)(F^{(2)}_{a^A_{1g}}-F^{(2)}_{a^B_{1g}})$ and $(F^{(2)}_{a^A_{1g}}-F^{(2)}_{a^B_{1g}})$ is, as clearly can be seen in Fig. 3, nonzero. The linear dichroism that branches from the cubic t_{2g} representation is shown in the middle panel. The second panel from the right shows the circular dichroic spectra. Differences in the antisymmetric part of the scattering tensor are almost always neglected, but for reasonable distortions, present in e.g., layered perovskite structures large differences can be seen between the $F^{(1)}_{b_{2u}}$ and $F^{(1)}_{e_u}$ spectra. Going beyond O_h symmetry thus also affects the antisymmetric part of F.

The middle panel of Fig. 3 shows the spectra of Mn^{3+} as a function of tetragonal distortion. Mn^{3+} has a d^4 configuration and depending on the distortion it will have an occupied $d_{x^2-y^2}$ orbital (top) or an occupied d_{z^2} orbital. As in the case of Ni^{2+}, for the spherical to cubic distortion, one has an immediate effect for all fundamental spectra and, in particular, also in the antisymmetric part of the scattering tensor. This is important for magnetic circular dichroism and RXD in all kinds of manganates where orbital order and magnetic order coexists.

The bottom panel of Fig. 3 shows the fundamental spectra of the scattering tensor for Cu^{2+} a d^9 configuration. This is a particularly simple and instructive example as all calculations can be done by hand and everything can be done in a one particle picture. The ground state has one hole in the d shell and the final state one hole in the $2p$ shell. The ground-state hole in the d shell will either be in the x^2-y^2 orbital (bottom of Fig. 3) or in the z^2 orbital (top of Fig. 3). For the natural dichroism (left panel, $F^{(0)}_{a^{xx}_{1g}}$ and $F^{(0)}_{a^{zz}_{1g}}$) one finds that for a $d_{x^2-y^2}$ hole the $F^{(0)}_{a^{zz}_{1g}}$ spectra are zero. This can be understood as one cannot excite into the $d_{x^2-y^2}$ hole with z polarized light. For a d_{z^2} hole there is a ratio of 1 to 3 for the different fundamental spectra. Note that the spectra are independent of the size of the distortion and only depend on the symmetry of the ground state. The symmetric part of the magnetic scattering tensor is zero for a d^9 configuration, which is a general property of any Kramers doublet. The spin-up and spin-down state are related by time-reversal symmetry and therefore should have the same symmetric part of the scattering tensor. At the same time the sum of the scattering tensor for the spin-up and spin-down state should be equal to the paramagnetic tensor which is given by the $F^{(0)}$ components. Therefore the symmetric magnetic part of the scattering tensor should be zero for a ground-state Kramers doublet. The antisymmetric part shows a very strong crystal orientation dependence. For a $d_{x^2-y^2}$ hole in the ground state, the $F^{(1)}_{a_{2u}}$ spectra is finite but the $F^{(1)}_{e_u}$ spectrum is zero. This is again related to the fact that one cannot excite into the $d_{x^2-y^2}$ hole with z polarized light.

When one now calculates the azimuthal dependence of a magnetic Bragg reflection at the Cu $L_{2,3}$ edge for real systems these big differences in the scattering tensor should lead to a huge difference in the scattered intensity between calculations in spherical symmetry and tetragonal symmetry. In Fig. 4 we show such calculations for $NaCu_2O_2$. This material shows a magnetic spiral with a wave factor of (0.5 0.227 0) in reciprocal lattice units. A possible magnetic structure, where all Cu atoms within the unit cell contribute constructively to the magnetic order at this wave vector is shown in the left panel of Fig. 4. In a Cartesian coordinate system the

scattering vector is given by $\hat{\boldsymbol{q}}=[0.721\ 0.692\ 0]$ and at the Cu L_3 edge $\theta'=41.4°$. We define $\boldsymbol{q}_\perp$ to be in the [001], which defines the experimental geometry as given in Eq. (13). The local spin direction depends on the position of the atom and can be written as $S=[0,\sin(r_q),\cos(r_q)]$ with r_q being the distance in the direction of $\boldsymbol{q}$ in units of the wave vector of the magnetic ordering. The difference between the scattered intensity as calculated in tetragonal or spherical symmetry is huge as can be seen in the left two panels of Fig. 4. We show calculations for incoming σ, π, polarized light, 45° linear-polarized rotated light ($\sigma+\pi$) and circular ($\sigma+\imath\pi$) polarized light. There is no simple relation between the calculations done in the artificially spherical symmetry and the calculations done in tetragonal symmetry. This could have been expected already due to the huge difference between $F^{(1)}_{e_u}$ and $F^{(1)}_{a_{2u}}$. The expression for the RXD intensity in spherical symmetry is proportional to $|F^{(1)}(\boldsymbol{\varepsilon}_{in}\times\boldsymbol{\varepsilon}^*_{out}\cdot\hat{\boldsymbol{m}})|^2$ [Eq. (14). or Hannon *et al.*[1]]. We have shown in Eq. (16) that in D_{4h} symmetry this should be $|F^{(1)}_{e_u}(\boldsymbol{\varepsilon}_{in}\times\boldsymbol{\varepsilon}^*_{out}\cdot\hat{\boldsymbol{m}}_{xy})+F^{(1)}_{a_{2u}}(\boldsymbol{\varepsilon}_{in}\times\boldsymbol{\varepsilon}^*_{out}\cdot\hat{\boldsymbol{m}}_z)|^2$. For the cuprates one finds that $F^{(1)}_{e_u}=0$. For the cuprates, the RXD spectra are thus only sensitive to the out-of-plane moment. This theoretical prediction has recently been experimentally confirmed by Leininger *et al.*[25] When orbital order is present it is for the determination of the magnetic structure with the use of RXD of extreme importance to consider the correct crystal symmetry when evaluating the magnetic scattered intensity.

V. CONCLUSION

We have shown that the fundamental spectra of the scattering or conductivity tensor are strongly influenced by the crystal-field symmetry at the transition metal $L_{2,3}$ edge. Both the symmetric part as noted previously[14–16] but also the antisymmetric part show strong deviations from the spectra calculated in spherical symmetry. When the symmetry is lowered the fundamental spectra known from spherical symmetry branch into several different spectra. At the same time higher-order spectra become nonzero and are important. In general more fundamental spectra are needed in order to describe the conductivity tensor as one might have expected. We have shown to what extent the crystal symmetry effects the magneto-optical effects and how they influence RXD and XAS experiments. The magnetization direction dependence of the conductivity tensor in our numerical examples is not due to magnetic anisotropy of the valence electrons. We neglected the 3*d* spin-orbit coupling and the spin is thus free to rotate. The anisotropy is induced by the spin-orbit coupling of the 2*p*-core-hole that couples via the Coulomb repulsion (direct as well as exchange part) with the valence electrons.

The reason for the deviations from the simple rule that the scattered intensity at an antiferromagnetic Bragg reflection is proportional to $|(\boldsymbol{\varepsilon}_{in}\times\boldsymbol{\varepsilon}^*_{out})\cdot\hat{\boldsymbol{m}}|^2$ is given by the fact that in spherical symmetry there is only one tensor element that describes the antisymmetric part of the conductivity tensor. In cubic symmetry this already becomes more complicated as $F^{(3)}$ cannot be neglected if S is larger then 1. In tetragonal or lower symmetry also $F^{(1)}$ branches to different spectra. When the spin aligns in a high-symmetry direction of the crystal there still will be only one tensor element describing the antisymmetric part of F and therefore the simple scattering rules as derived in spherical symmetry will still hold. Even when this tensor element is made from a linear combination of $F^{(1)}$ and $F^{(3)}$; as long as their ratio is the same for all polarizations the simple rules hold. In most cases the, single ion anisotropy will dictate the preferred direction of the magnetic moments, aligning it along high symmetry directions. In this case the simple rules are valid.

Local magnetic moments are not always aligned in a high-symmetry crystal direction. Well known examples are the simple rocksalts such as NiO, MnO, and CoO. An other class would be magnetic spiral structures as found in the cuprates and manganates. In these cases a more involved spectral line-shape analysis is needed in order to determine the magnetization direction. One then cannot measure the scattered intensity at a single photon energy, but needs to measure the energy dependence at all azimuthal directions in order to obtain more information. By comparing the line shape to theory at different azimuthal directions or by the use of sum rules one then can still obtain the full information as present in the data.

The present calculations could be proved by magnetic circular and linear dichroism experiments. Temperature dependence of the magneto-optical effects as well as nonfull magnetization of the sample will be discussed in a future work.

ACKNOWLEDGMENTS

The research in Köln is supported by the Deutsche Forschungsgemeinschaft through Grant No. SFB 608 and the Cologne Bonn Graduate School.

APPENDIX: RELATION TO SPHERICAL TENSORS FORMALISM

Within the current paper, we have expressed the scattering tensor as a 3×3 matrix on a basis of linear x, y, and z polarized light. This is the standard notation as used within modern optical theory.[29–31] For core level spectroscopy there are however several theoretical works that use a coupling of spherical tensors as presented by Luo *et al.*[45] Within this appendix we will present a relation between these two notations. As within the rest of the paper we restrict ourselves to dipole excitations only. First of all one can change the basis of the scattering tensor from linear polarized light to circular polarized light by a unitary transformation: $x=(l-r)/\sqrt{(2)}$, $y=\imath(l+r)/\sqrt{(2)}$, $z=z$. The basis set of circular polarized light represents an angular momentum vector with l, z, and r equal to $m_l=-1$, $m_l=0$, and $m_l=1$, respectively. One can couple the angular momentum vector of the incoming and outgoing light (left and right hand side of the scattering tensor) to a single vector of angular momentum $L=0$, 1, and 2. This again represents nine components for the scattering tensor ($L=0$ has one element, $L=1$ has three elements with different M_L values, and $L=3$ has five elements with different M_L values). The relation between F_{L,M_L} and F_{ij} with i, $j\in\{x,y,z\}$ is

$$F_{0,0} \propto F_s = \frac{1}{3}(F_{xx} + F_{yy} + F_{zz}),$$

$$\sqrt{\frac{1}{2}}(F_{1,-1} - F_{1,1}) \propto F_{p,x} = \frac{1}{2}(F_{yz} - F_{zy}),$$

$$\imath\sqrt{\frac{1}{2}}(F_{1,-1} + F_{1,1}) \propto F_{p,y} = \frac{1}{2}(F_{zx} - F_{xz}),$$

$$F_{1,0} \propto F_{p,z} = \frac{1}{2}(F_{xy} - F_{yx}),$$

$$\imath\sqrt{\frac{1}{2}}(F_{2,-1} + F_{2,1}) \propto F_{d,yz} = \frac{1}{2}(F_{yz} + F_{zy}),$$

$$\sqrt{\frac{1}{2}}(F_{2,-1} - F_{2,1}) \propto F_{d,xz} = \frac{1}{2}(F_{zx} + F_{xz}),$$

$$\imath\sqrt{\frac{1}{2}}(F_{2,-2} - F_{2,2}) \propto F_{d,xy} = \frac{1}{2}(F_{xy} + F_{yx}),$$

$$F_{2,0} \propto F_{d,z^2-1/3} = F_{zz} - F_s,$$

$$\sqrt{\frac{1}{2}}(F_{2,-2} + F_{2,2}) \propto F_{d,x^2-y^2} = F_{xx} - F_{yy}. \quad \text{(A1)}$$

In Eq. (2) we expand the scattering tensor on the local magnetization direction. This can naturally be done for either of the two formulations of the polarization. In spherical symmetry there is a particular simple relation between the scattering tensor expanded on the magnetization direction and the coupling of the polarization in spherical tensors. One knows that by symmetry the scattering tensor should transform the same as the coupled polarization vectors and thus the scattering vectors expanded on spherical tensors: F^{km}_{L,M_L} are only nonzero for $L=k$ and $M_L=m$. One furthermore knows that $F_{L,M_L}=F_{L,M'_l}$ which then defines Eq. (5).

When the crystal symmetry is considered, and the calculations are not done in spherical symmetry, angular momentum is not strictly conserved for the electrons only (one can transfer angular momentum to the entire crystal). This allows F_{L,M_L} components to depend on the expansion of the magnetization direction with $L \neq k$. In the coupled tensor notation $F_{L=2,M_L}$ components do contain the natural linear dichroism. The expansion coefficients in the magnetization direction with $k \neq 0$ however do all vanish for a paramagnetic sample as the full angular integral over a spherical harmonic for all but the spherical harmonic with $k=0$ equal to zero. The $F^{(k=2)}_{ij}$ components therefore only include magnetic linear dichroism and no natural linear dichroism. The natural linear dichroism is all contained in the different $F^{(k=0)}_{ij}$ components. The $F_{L=2,M_L}$ components in tetragonal and lower symmetry do depend also on $k=0$ expansions in the magnetization direction. By expanding the scattering tensor strictly on the magnetization direction one can separate the natural and magnetic linear dichroism. The fundamental spectra as defined in this paper are not equivalent to tensor elements of the scattering tensor but describe the magnetization direction dependence of the scattering tensor. In spherical symmetry this is equivalent but for real crystal symmetries there are more expansion coefficients that determine a single scattering tensor element.

[1] J. P. Hannon, G. T. Trammell, M. Blume, and Doon Gibbs, Phys. Rev. Lett. **61**, 1245 (1988).
[2] M. Blume, J. Appl. Phys. **57**, 3615 (1985).
[3] P. M. Platzman and N. Tzoar, Phys. Rev. B **2**, 3556 (1970).
[4] F. de Bergevin and M. Brunel, Acta Crystallogr., Sect. A: Cryst. Phys., Diffr., Theor. Gen. Crystallogr. **37**, 314 (1981).
[5] M. Blume and D. Gibbs, Phys. Rev. B **37**, 1779 (1988).
[6] S. W. Lovesey, J. Phys. C **20**, 5625 (1987).
[7] P. Rennert, Phys. Rev. B **48**, 13559 (1993).
[8] J. P. Hill and D. F. McMorrow, Acta Crystallogr., Sect. A: Found. Crystallogr. **52**, 236 (1996).
[9] See Hannon *et al.* (Ref. 1) and articles citing this paper.
[10] P. Carra and B. T. Thole, Rev. Mod. Phys. **66**, 1509 (1994).
[11] S. Di Matteo, Y. Joly, A. Bombardi, L. Paolasini, F. de Bergevin, and C. R. Natoli, Phys. Rev. Lett. **91**, 257402 (2003).
[12] N. Stojić, N. Binggeli, and M. Altarelli, Phys. Rev. B **72**, 104108 (2005).
[13] R. G. Newton, Am. J. Phys. **44**, 639 (1976).
[14] E. Arenholz, G. van der Laan, R. V. Chopdekar, and Y. Suzuki, Phys. Rev. B **74**, 094407 (2006).
[15] E. Arenholz, G. van der Laan, R. V. Chopdekar, and Y. Suzuki, Phys. Rev. Lett. **98**, 197201 (2007).
[16] G. van der Laan, E. Arenholz, R. V. Chopdekar, and Y. Suzuki, Phys. Rev. B **77**, 064407 (2008).
[17] J. Kuneš and P. M. Oppeneer, Phys. Rev. B **67**, 024431 (2003).
[18] P. M. Oppeneer, T. Kraft, and H. Eschrig, Phys. Rev. B **52**, 3577 (1995).
[19] Yu. A. Uspenskii, E. T. Kulatov, and S. V. Halilov, Phys. Rev. B **54**, 474 (1996).
[20] S. Uba, A. N. Yaresko, L. Uba, A. Ya. Perlov, V. N. Antonov, R. Gontarz, and H. Ebert, Phys. Rev. B **57**, 1534 (1998).
[21] G. van der Laan and E. Arenholz, Eur. Phys. J. Spec. Top. **169**, 187 (2009).
[22] Within this paper, the notation $[x,y,z]$ is used to define a vector in real space Cartesian coordinates. The vector $[x,y,z]$ is thus not necessarily equal to the vector $x\boldsymbol{a}+y\boldsymbol{b}+z\boldsymbol{c}$ with $\boldsymbol{a}$, $\boldsymbol{b}$, and $\boldsymbol{c}$ the primitive vectors spanning the Bravis lattice.
[23] I. P. Krug, F. U. Hillebrecht, H. Gomonaj, M. W. Haverkort, A. Tanaka, L. H. Tjeng, and C. M. Schneider, EPL **81**, 17005 (2008).
[24] I. P. Krug, F. U. Hillebrecht, M. W. Haverkort, A. Tanaka, L. H. Tjeng, H. Gomonay, A. Fraile-Rodríguez, F. Nolting, S. Cramm, and C. M. Schneider, Phys. Rev. B **78**, 064427 (2008).
[25] Ph. Leininger, M. Rahlenbeck, M. Raichle, B. Bohnenbuck,

A. Maljuk, C. T. Lin, B. Keimer, E. Weschke, E. Schierle, S. Seki, Y. Tokura, and J. W. Freeland, Phys. Rev. B **81**, 085111 (2010).
[26] F. M. F. de Groot and A. Kotani, *Core Level Spectroscopy of Solids* (CRC Press, New York, 2008).
[27] C. J. Ballhausen, *Introduction to Ligand Field Theory* (McGraw-Hill, New York, 1962).
[28] A. Abragam and B. Bleaney, *Electron Paramagnetic Resonance of Transition Ions* (Clarendon, Oxford, England, 1970).
[29] L. D. Landau, E. M. Lifshitz, and L. P. Pitaevskii, *Electrodynamics of Continuous Media* (Elsevier, Amsterdam, 1984).
[30] R. M. A. Azzam and N. M. Bashara, *Ellipsometry and Polarized Light* (Elsevier, Amsterdam, 1977).
[31] G. R. Fowles, *Introduction to Modern Optics* (Dover, New York, 1989).
[32] G. Subías, J. Herrero-Martín, J. García, J. Blasco, C. Mazzoli, K. Hatada, S. Di Matteo, and C. R. Natoli, Phys. Rev. B **75**, 235101 (2007).
[33] M. W. Haverkort, S. I. Csiszar, Z. Hu, S. Altieri, A. Tanaka, H. H. Hsieh, H.-J. Lin, C. T. Chen, T. Hibma, and L. H. Tjeng, Phys. Rev. B **69**, 020408 (2004).
[34] F. M. F. de Groot, J. C. Fuggle, B. T. Thole, and G. A. Sawatzky, Phys. Rev. B **42**, 5459 (1990).
[35] A. Tanaka and T. Jo, J. Phys. Soc. Jpn. **63**, 2788 (1994).
[36] R. Rückamp, E. Benckiser, M. W. Haverkort, H. Roth, T. Lorenz, A. Freimuth, L. Jongen, A. Möller, G. Meyer, P. Reutler, B. Büchner, A. Revcolevschi, S.-W. Cheong, C. Sekar, G. Krabbes, and M. Grüninger, New J. Phys. **7**, 144 (2005).
[37] G. Ghiringhelli, M. Matsubara, C. Dallera, F. Fracassi, R. Gusmeroli, A. Piazzalunga, A. Tagliaferri, N. B. Brookes, A. Kotani, and L. Braicovich, J. Phys.: Condens. Matter **17**, 5397 (2005).
[38] G. Ghiringhelli, M. Matsubara, C. Dallera, F. Fracassi, A. Tagliaferri, N. B. Brookes, A. Kotani, and L. Braicovich, Phys. Rev. B **73**, 035111 (2006).
[39] S. I. Csiszar, M. W. Haverkort, Z. Hu, A. Tanaka, H. H. Hsieh, H.-J. Lin, C. T. Chen, T. Hibma, and L. H. Tjeng, Phys. Rev. Lett. **95**, 187205 (2005).
[40] M. W. Haverkort, Z. Hu, J. C. Cezar, T. Burnus, H. Hartmann, M. Reuther, C. Zobel, T. Lorenz, A. Tanaka, N. B. Brookes, H. H. Hsieh, H.-J. Lin, C. T. Chen, and L. H. Tjeng, Phys. Rev. Lett. **97**, 176405 (2006).
[41] K. W. Edmonds, G. van der Laan, A. A. Freeman, N. R. S. Farley, T. K. Johal, R. P. Campion, C. T. Foxon, B. L. Gallagher, and E. Arenholz, Phys. Rev. Lett. **96**, 117207 (2006).
[42] M. W. Haverkort, Z. Hu, A. Tanaka, G. Ghiringhelli, H. Roth, M. Cwik, T. Lorenz, C. Schüßler-Langeheine, S. V. Streltsov, A. S. Mylnikova, V. I. Anisimov, C. de Nadai, N. B. Brookes, H. H. Hsieh, H.-J. Lin, C. T. Chen, T. Mizokawa, Y. Taguchi, Y. Tokura, D. I. Khomskii, and L. H. Tjeng, Phys. Rev. Lett. **94**, 056401 (2005).
[43] E. Pavarini, S. Biermann, A. Poteryaev, A. I. Lichtenstein, A. Georges, and O. K. Andersen, Phys. Rev. Lett. **92**, 176403 (2004).
[44] P. Kuiper, J.-H. Guo, Conny Såthe, L.-C. Duda, J. Nordgren, J. J. M. Pothuizen, F. M. F. de Groot, and G. A. Sawatzky, Phys. Rev. Lett. **80**, 5204 (1998).
[45] J. Luo, G. T. Trammell, and J. P. Hannon, Phys. Rev. Lett. **71**, 287 (1993).